SASEC
1st Southern African Solar Energy Conference
21-23 May 2012

A WIND LOADING CORRELATION FOR AN ISOLATED SQUARE HELIOSTAT, PART 1: LIFT AND DRAG FORCES

Thomas H Roos[1]

[1] CSIR, P O Box 395, Pretoria, 0001, South Africa; Phone: +27 12 841-2329; Fax: +27 12 349-1156; E-Mail: throos@csir.co.za

Abstract

A design requirement of a heliostat is the ability to withstand storm loads in the stow position and operational wind loads in any position. To design a heliostat, therefore, one must be able to predict the wind loading on the heliostat for all elevation angles of the heliostat and all wind directions relative to the heliostat coordinate system. Fortunately, experimental wind tunnel force and moment coefficient data in the x, y and z directions exist in tabular format for an isolated heliostat, and are in the public domain, but still require interpolation between different points in a large dataset. This paper shows that the data points fit definable patterns, allowing the use of Fourier analysis to fit a small number of correlations to describe the entire dataset to high accuracy. Correlations for the lift and drag forces are presented. A companion paper presents correlations for the side forces and correlations for moments about the three principal axes, and discusses the behavior of the correlations.

Keywords: heliostat; wind; loading; lift; drag; force; correlation

1. Introduction

One of the design requirements of a heliostat is the ability to withstand three types of wind loads [1]:

- Storm winds: in discrete, infrequent storm loads of up to 40m/s freestream wind speed, heliostat in *stowed* position must survive (no static failure or low cycle fatigue failure),
- Moderate winds: at wind speeds up to 22m/s freestream, a heliostat in *any* position must survive (no static failure or low cycle fatigue failure), and the actuation mechanisms must be able to move the heliostat to the stow position in preparation for possible storm winds, and
- Operational winds: at more frequent oscillating wind speeds up to 15m/s freestream, the actuation mechanisms must be capable to allow a heliostat in *any* position to track the sun accurately, and the resultant loads should not lead to high cycle fatigue failure.

In the above, freestream values are measured at 10m above ground. To design a heliostat, therefore, one must be able to predict the mean and oscillating wind loads on the heliostat for all elevation angles of the heliostat and all wind directions relative to the heliostat coordinate system.

This is usually done using experimental measurements on scale models in atmospheric wind tunnels, and with numerical simulations (steady-state and transient) using computational fluid dynamics (CFD) providing additional insight. An example of such a study is given by Huss *et al* [2]. It is important to obtain the correct boundary conditions for both techniques in such analyses: velocity and turbulence profiles must match the true, full-scale conditions, including the power spectra in the case of the wind tunnel tests. Such an experimental dataset is expensive to generate, (and when performed is understandably proprietary) presenting a barrier to entry for researchers. Fortunately, one experimental wind tunnel dataset for an isolated square heliostat exists and is in the public domain [3]. Isolated heliostat loading data is sufficient for structural design purposes, rather than data for one in a field. The interaction of winds with a heliostat field is shown schematically in Figure 1, where turbulent boundary layer winds are shown approaching a field on the left and within the field on the right. As a consequence of wind impingement on upwind heliostats in a heliostat field, a decrease of mean wind speed over the height of the heliostats is caused within the field, leading to heliostats interior to the field experiencing lower mean wind loads and often decreased fluctuations in wind load about the mean, relative to heliostats at the edge of the field [3].

This dataset comprises some 2000 points of interest, making interpolation difficult. A coherent set of correlation curves fitted to the data would simplify this challenge, and identify outliers in the data. This

paper describes the method followed to fit correlations to this large dataset, and presents the correlations for the principal forces (lift and drag). A companion paper [4] will present correlations for the side forces, correlations for moments about the three principal axes, and discuss the behavior of the correlations.

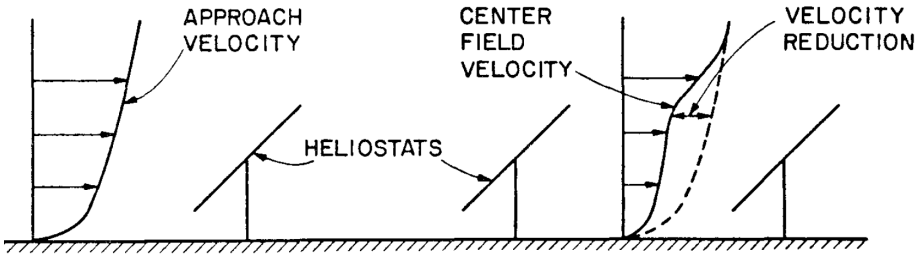

Figure 1: Velocity reductions within a field of heliostats [3]

2. Experimental dataset of Peterka *et al* [3]

2.1. Test description

Wind tunnel tests were performed on a square isolated heliostat model placed in a dedicated atmospheric boundary layer wind tunnel [3], which creates a velocity and turbulence profile upstream of the model similar to full-scale representative conditions (see Figure 2 left and centre). This turbulent boundary layer has been shown to model the atmosphere boundary layer for model scales smaller than about 1:100. The heliostat model is at 1/60th scale (see Figure 3), however, and for this scale the wind-tunnel does not adequately simulate the lower frequency gustiness due to the limitation of the tunnel cross section size (see Figure 2 right), and at a 1:60 scale the larger turbulence scales are not completely represented. This should not affect mean wind load measurements but can result in underestimation of peak fluctuating wind load on the heliostat from the lack of the low-frequency spectral content [3]. The wind-tunnel Reynolds number was approximately 30 000 – 70 000 at the testing wind speeds used for this study, thus achieving Reynolds number independence of the aerodynamic coefficient.

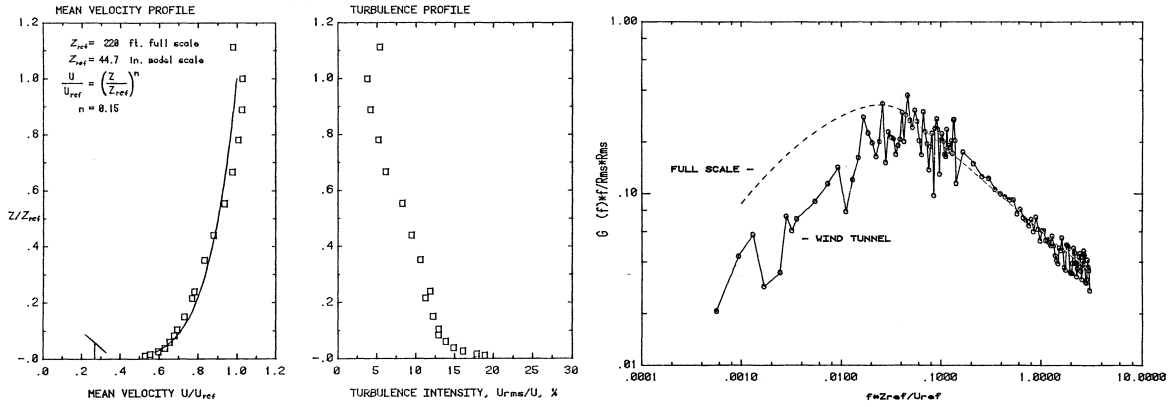

Figure 2: Vertical distributions of velocity (left) and turbulence (centre), and power spectrum of turbulence (right) generated in the wind tunnel [3]

The model was fitted with a 6-component balance, placed on a turntable within the wind tunnel and the azimuth and elevation angles were varied relative to the oncoming wind (see Figure 3). Each test run lasted 32 seconds, representing 10 to 30 minutes when scaled to full-size, the average length of a thunderstorm. The sign convention is that used by Peterka et al [3] illustrated in Figure 3 (right): the heliostat azimuth angle is measured anticlockwise from east and in all cases is 270˚ (y-axis runs due east, x-axis runs due south). The wind direction (θ) is measured clockwise from north (0˚) to south (180˚). While the heliostat elevation angle (EL) is measured from the vertical in the Peterka *et al* [3] sign convention, in this paper this convention is replaced with angle of attack (α), measured from horizontal (0° represents horizontal, 90° vertical).

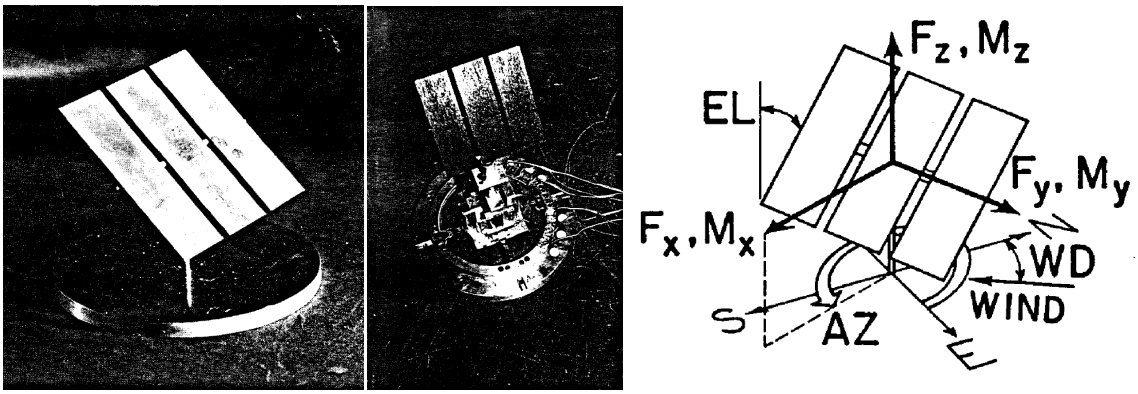

Figure 3: 1/60th scale heliostat (left), model on 6 component balance (mid), axis convention (right) [3]

During each test, forces and moments in the three axes were continuously measured and recorded. Thereafter they were non-dimensionalised to coefficient form:

$$CF_{x,y,z} = \frac{F_{x,y,z}}{\left(\frac{\rho U_{ref}^2}{2}\right)A_{ref}} \quad \text{and} \quad CM_{x,y,z} = \frac{M_{x,y,z}}{\left(\frac{\rho U_{ref}^2}{2}\right)A_{ref}L_{ref}}$$

where *CF* and *CM* are the non-dimensionalised force and moment coefficients, $F_{x,y,z}$ is the component of force [N] in x, y and z direction respectively, $M_{x,y,z}$ is the moment [N.m] about the *x*, *y* and *z* axes respectively, □ is the density of air [kg.m^{-3}], U_{ref} is upstream freestream velocity [m.s^{-1}], A_{ref} is the heliostat surface reference area [m^2] and L_{ref} is the heliostat reference length [m]. The maximum, minimum, mean, root mean squared (RMS), gust factor $\left(Gfact = \frac{peak}{mean}\right)$ and peak factor $\left(Pfact = \frac{(peak-mean)}{RMS}\right)$ values of the *CF* and *CM* values were then tabulated. Here *peak* refers to the greater of the absolute value of the maximum and minimum values.

2.2. Data quality and resolution control[1]

Unfortunately, the data was published as a fixed fraction to only two decimal places. In cases where the heliostat is near horizontal, the mean and RMS coefficient values contain only one significant digit which is often 1, providing unacceptably low resolution. Table 1 demonstrates this, showing the original published CF_x values for α = 0˚. Fortunately, in all cases the *Pfact* and *Gfact* ratios are given with three significant digits. This fact was used to generate higher resolution values for the mean and RMS coefficients, as follows:

$$Pfact = \frac{(peak - mean)}{RMS} = \frac{peak\left(1 - \frac{mean}{peak}\right)}{RMS} = \frac{peak\left(1 - \frac{1}{Gfact}\right)}{RMS}$$

$$\therefore RMS = \frac{peak\left(1-\frac{1}{Gfact}\right)}{Pfact}, \quad \text{and} \quad mean = \frac{peak}{Gfact}$$

Using the *Pfact* and *Gfact* relationships described above, the mean and RMS values can be determined to more significant digits, increasing resolution. To do this a higher resolution peak value is required, as the examples in Table 1 show peak values resolved to one or at best two significant figures, with a minimum magnitude of 0.05 (at least has a five times the RMS value). For θ values from 0˚ to 90˚, the peak value is the maximum, while for 112.5˚ to 180˚ the peak value is the minimum. The approach followed was to find the highest peak value (to be conservative) with three digits after the decimal point that simultaneously 1) rounds to the same two-decimal point value published by Peterka et al [3], and 2) generates RMS and mean

[1] The PDF version of Peterka et al [3] available at the websites listed in the references is an electronic scan of the original typed hard copy, and is of poor quality in places, making interpretation of the text difficult. The data was thus plotted to ensure integrity (e.g. identifying if a minus sign exists in the data but cannot be discerned from the text quality, discerning between 1 and 4 and between 0 and 8 for doubtful characters).

values that in turn round to the same two-decimal point values published [3].

Variable	Wind direction □ (°)								
	0	22.5	45	67.5	90	112.5	135	157.5	180
Mean	0.06	0.07	0.05	0.03	0.01	-0.02	-0.04	-0.05	-0.05
Max	0.12	0.13	0.10	0.07	0.05	0.01	0.01	0.00	0.00
Min	0.02	0.02	0.00	-0.01	-0.01	-0.05	-0.09	-0.10	-0.11
RMS	0.01	0.02	0.01	0.01	0.01	0.01	0.01	0.02	0.01
Gfact	1.92	1.86	2.06	2.41	3.68	3.04	2.20	2.01	2.48
Pfact	3.87	3.78	3.97	3.43	4.95	3.63	3.84	3.33	4.45

Table 1: Original low resolution CF_x data for □ = 0° [3]

This is illustrated in Table 2. *Pfact* and *Gfact* ratios are not given as they are unchanged. The bold, underlined figures are the values chosen from either the maximum or minimum as peak values, and each have at least three digits after the decimal point, giving at least two significant figures. Using the *Pfact* and *Gfact* relationships, the mean and RMS values have been regenerated to at least three significant figures each (wind directions 0° and 180° each have RMS values to four significant figures to show that they round to the original published value of 0.01). This method was applied to all the published data for completeness.

Variable	Wind direction □ (°)								
	0	22.5	45	67.5	90	112.5	135	157.5	180
Mean	0.0630	0.0720	0.0505	0.0307	0.0147	-0.0178	-0.0427	-0.0517	-0.0451
Max	**0.121**	**0.134**	**0.104**	**0.074**	**0.054**	0.01	0.01	0.00	0.00
Min	0.02	0.02	0.00	-0.01	-0.01	**-0.054**	**-0.094**	**-0.104**	**-0.1118**
RMS	0.01498	0.0164	0.0135	0.0126	0.0079	0.00998	0.0134	0.0157	0.01499

Table 2: *CFx* data with improved resolution of RMS and mean values

2.3. Pattern recognition

For each heliostat setting angle (α) position and approach wind angle (θ), 24 values are of interest: 6 coefficients (CF_x, CF_y, CF_z, CM_x, CM_y and CM_z) for which 4 values each are necessary: maximum, minimum, mean and RMS. 6 heliostat setting angles (α = 0°, 3°, 6°, 10°, 45°, 90°) have been tested at 9 wind directions (θ = 0°, 22.5°, 45°, 67.5°, 90°, 112.5°, 135°, 157.5° and 180°), while a further 4 heliostat setting angles (α = 15°, 30°, 60° and 75°) have been tested at only 5 wind directions (θ = 0°, 45°, 90°, 135°, and 180°). This gives $24 \times ((6\times9) + (4\times5)) = 1776$ points of interest, which is a formidable data management and interpolation challenge. With a dataset of this size, a coherent set of correlation curves fitted to the data would simplify this challenge, and identify outliers in the data. Fitting such correlations to the data requires the recognition and exploitation of patterns within the dataset.

The 1st pattern recognized was that the values of the ratio $Pfact = \frac{(peak-mean)}{RMS}$ fluctuate around 4 for all the *CF* and *CM* values. If the RMS value is regarded as a standard deviation (σ), it therefore follows that the data distribution can be considered to be similar to a normal distribution, with the peak (maximum for positive, minimum for negative) about four standard deviations from the mean[2]. It can be seen in Table 1

[2] For a normal distribution the fraction of the data values lying within 1, 2, 3 and 4 standard deviations symmetrically distributed on either side of the mean are 68%, 95%, 99.7% and 99.994% respectively.

that the maximum and minimum values are not always exactly equidistant from the mean value. If the distribution of the data is assumed to be normal, however, with the distance from the mean value to the maximum and minimum values made equal to that to the peak value, the resulting correlation would be conservative. So, instead of correlating the mean, maximum and minimum values, it is only necessary to correlate the mean and RMS value distributions (since $max_{corr} = mean_{corr} + Pfact \times RMS_{corr}$ and $min_{corr} = mean_{corr} - Pfact \times RMS_{corr}$), and to assume that $Pfact = 4$. This halves the data load.

The 2nd pattern recognized was that at any given heliostat setting angle, the variation in the mean and RMS values of *CF* and *CM* can be described by a combination of trigonometric functions as a function of θ, using Fourier analysis:

$$f(\theta) = c + \sum_{i=1}^{N} (a_i \sin(i\theta) + b_i \cos(i\theta))$$

This is physical, as the loading is related at least to first order to the projected heliostat area seen by the wind, which is described by sine and cosine relationships depending on the force considered. Fitting correlation curves in this manner allows data subsets consisting of 9 wind directions to be compared to those consisting of 5 wind directions.

3. Correlation curve fitting

3.1. $CF_{x\ mean}$

As can be seen in Figure 4, the $CF_{x\ mean}$ curves strongly resemble the cosine function (full positive force in x direction for wind direction of 0°, full negative force in negative x direction for wind direction of 180°, and near zero force in x direction with wind direction of 90°). A better fit to the data is however obtained using the square root of the cosine of the wind angle θ, or:

$$CF_{x\ mean}(\alpha, \theta) = C_1(\alpha) \times \sqrt{\cos\theta} + C_2(\alpha)$$

To allow meaningful results for wind directions of 90° < θ < 270°, this is replaced by the more general expressions

$$CF_{x\ mean}(\alpha, \theta) = C_1(\alpha) \times \left(\frac{\cos\theta}{\sqrt{|\cos\theta|}}\right) + C_2(\alpha)$$

C_1 and C_2 are correlated by the expressions:

0° ≤ α ≤ 15°: $$C_1(\alpha) = 0.05594 + \frac{(\alpha - 0)}{(15 - 0)} \times (0.15079 - 0.05594)$$

15° < α ≤ 90°: $$C_1(\alpha) = 0.24237 - 0.12703 \times \cos(2\alpha) + 0.13109 \times \sin(2\alpha)$$
$$-0.58076 \times \cos\alpha + 1.14064 \times \sin\alpha$$

and

$$C_2(\alpha) = -0.005051 + 0.0001090 \times \alpha$$

3.2. $CF_{x\ RMS}$

The $CF_{x\ RMS}$ curves (not shown) are largely symmetrical about α = 90°, resemble $|\cos\theta|$ in shape, and scale approximately linearly with elevation angle α (as do the $CF_{x\ mean}$ curves). If the RMS values are divided by the C_1 data values mentioned above, the results nearly collapse onto a single curve of the form:

$$\frac{CF_{x\ RMS}(\alpha, \theta)}{C_1(\alpha)} = C_3(\alpha) \times |\cos\theta| + C_4(\alpha)$$

The C_3 and C_4 distributions are correlated by:

$$C_3(\alpha) = -0.00044494 \times \alpha + 0.116297$$

$$C_4(\alpha) = -0.000606747 \times \alpha + 0.153464$$

The $CF_{x\,RMS}$ values can then be calculated:

$$CF_{x\,RMS}(\alpha,\theta) = C_1(\alpha)\times[C_3(\alpha)\times|\cos\theta| + C_4(\alpha)]$$

Using the previously calculated values of $CF_{x\,mean}$ and assuming $Pfact = 4$, values of $CF_{x\,max}$ and $CF_{x\,min}$ as a θ and α can be calculated from

$$CF_{x\,max}(\alpha,\theta) = CF_{x\,mean}(\alpha,\theta) + 4\times CF_{x\,RMS}(\alpha,\theta)$$

$$CF_{x\,min}(\alpha,\theta) = CF_{x\,mean}(\alpha,\theta) - 4\times CF_{x\,RMS}(\alpha,\theta)$$

3.3. $CF_{z\,mean}$

While not discernable for α = 0° and α = 90°, the $CF_{z\,mean}$ curves also have a cosine shape as can be seen in Figure 4 as well as in the curves at other values of α not shown. In this case, the shape of the data distribution is however better correlated by the cube root of the cosine of the wind angle θ, or:

$$CF_{z\,mean}(\alpha,\theta) = C_5(\alpha)\times\left(\frac{\cos\theta}{\sqrt[3]{|\cos\theta|}}\right) + C_6(\alpha)$$

The C_5 correlation consists of three sections, two linear and one trigonometric:

0° ≤ α ≤ 6°: $C_5(\alpha) = -0.01338 + \frac{(\alpha-0)}{(6-0)}\times(0.23582 + 0.01338)$

6° ≤ α ≤ 30°: $C_5(\alpha) = 0.23582 + \frac{(\alpha-0)}{(30-0)}\times(0.827332 - 0.23582)$

30° < α ≤ 90°: $C_5(\alpha) = 0.43416\times\cos\alpha + 0.53089\times\sin(2\alpha) - 0.014772$

C_6 is given by a simple linear correlation:

$$C_6(\alpha) = 0.0037246 - 0.00056640\times\alpha$$

3.4. $CF_{z\,RMS}$

The $CF_{z\ RMS}$ curves (not shown) resemble $|\cos\theta|$ in shape (like the $CF_{x\ RMS}$ curves) but are not very symmetrical about α = 90°, and do not display a large dependency on heliostat setting angle α. The pattern of the graphs is well represented by:

$$CF_{z\,RMS}(\alpha,\theta) = C_7(\alpha)\times|\sin(2\theta)| + C_8(\alpha)\times|\cos\theta| + C_9(\alpha)\times\cos\theta + C_{10}(\alpha)$$

C_7 to C_{10} are correlated by linear interpolations between values at discrete α points given in Table 3.

Angle(°)	C_7	C_8	C_9	C_{10}
0	0.017188	-0.0078651	0.00090260	0.052855
10	0.010067	-	-	-
15	-	-	-0.00245896	-
30	-	0.085795	-	-
45	0.024131	-	-	-
60	-	-	-	0.051271
75	-	-	-0.013720	-
90	0.001521	0.0063273	0.0067000	0.013562

Table 3: Interpolation points for C_7 to C_{10}

As with the CF_x case, values of $CF_{z\,max}$ and $CF_{z\,min}$ as a function of θ and α can be calculated from

$$CF_{z\,max}(\alpha,\theta) = CF_{z\,mean}(\alpha,\theta) + 4\times CF_{z\,RMS}(\alpha,\theta)$$

$$CF_{z\,min}(\alpha,\theta) = CF_{z\,mean}(\alpha,\theta) - 4\times CF_{z\,RMS}(\alpha,\theta)$$

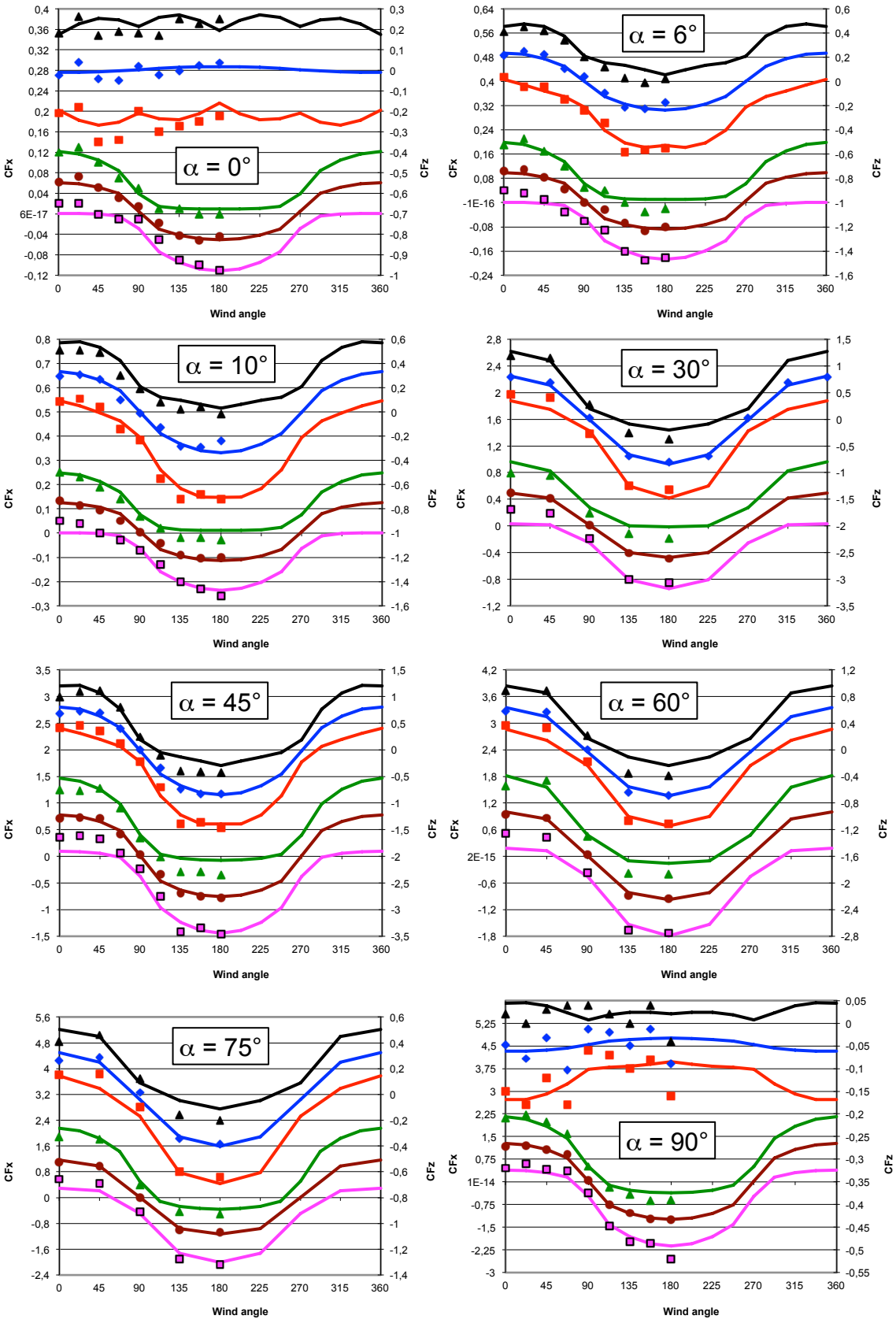

Figure 4: Comparison of data (markers) and correlations (lines) for CF_x min, mean and max (bottom 3 in each chart) and CF_z min, mean and max (top 3 in each chart) plotted versus □, for 8 values of □

4. Discussion

Examining all the predicted curves (not just those displayed in Figure 4), the $CF_{x\,mean}$ correlation is a good fit, and is nearly always conservative except for $\alpha = 0°$ and $\alpha = 6°$ at where the experimental values peak at $\theta = 22.5°$ instead of at $\theta = 0°$. Here they exceed the curve fit values by 22% and 14% respectively, and the experimental values at $\theta = 0°$ by 12.5% and 5.8% respectively. The $CF_{x\,max}$ and $CF_{x\,min}$ correlations provide a good fit, and are nearly always conservative except (as in the $CF_{x\,mean}$ correlation) at $\alpha = 0°$ and $\alpha = 6°$, where the values peak at for $\theta = 22.5°$ instead of at $\theta = 0°$. The apparent exceptions for $CF_{x\,min}$ at $\theta = 180°$ at $\alpha = 10°$ and $\alpha = 90°$ are explained by the experimental data having $Pfact$ values of 5.33 and 5.37 respectively. $Pfact$ values of 4 in these instances would have yielded experimental $CF_{x\,min}$ values of -0.223 and -2.232 (instead of -0.26 and -2.56) respectively, much closer to the respective correlation values of -0.2366 and -2.1208.

Disregarding $\alpha = 0°$ and $\alpha = 90°$ where the peak-to-trough experimental range is less than 0.1, the $CF_{z\,mean}$ correlation provides a good fit, and is nearly always conservative except at $\alpha = 6°$ where the experimental value peaks at $\theta = 22.5°$ instead of at $\theta = 0°$, exceeding the correlation by 12.6% and the experimental value at $\theta = 0°$ by 14.1%. Except at $\alpha = 0°$ and $\alpha = 90°$, the $CF_{z\,max}$ and $CF_{z\,min}$ correlations provide a good fit and are nearly always conservative. The exceptions for $CF_{z\,min}$ at $\theta = 350°$ (experimental values of $CF_{z\,min}$ of -0.58 and -0.72 at $\alpha = 6°$ and $\alpha = 10°$ respectively) are partly explained by the experimental data having $Pfact$ values of 4.39 and 4.54 respectively. $Pfact$ values of 4 in these instances would have yielded experimental $CF_{x\,min}$ values of -0.549 and -0.672 respectively, about midway between the current values and the respective correlation values of -0.506 and -0.630.

Finally, as discussed in section 2.1, the fact that the lower frequency gustiness is not completely represented at 1:60 scale should not affect mean wind load measurements but can result in underestimation of peak fluctuating wind load on the heliostat from the lack of the low-frequency spectral content [3]. This can be compensated for by increasing $Pfact$ values in the correlations above 4 when analyzing oscillating loads.

5. Conclusion

Correlations have been presented for lift (CF_z) and drag (CF_x) wind forces on an isolated square heliostat with good fit, producing accurate or at least conservative predictions. These correlations should be useful in heliostat preliminary design studies where the environment matches the modelling assumptions: flat terrain with developed turbulent oncoming wind profile.

Acknowledgements

The author would like to thank CSIR R&D office for directly supporting this work.

References

[1] Strachan J. W. and Houser R. M., (1993), "Testing and Evaluation of Large-Area Heliostats for Solar Thermal Applications", Sandia Laboratories Report SAND92-1381

[2] Huss S., Traeger Y.D., Shvets Z., Rojansky M., Stoyanoff S. and Garber J., (2011), "Evaluating Effects of Wind Loads in Heliostat Design", Proceedings of SolarPACES2011, Granada, Spain, September 2011

[3] Peterka J.A., Hosoya N., Bienkiewicz B. and Cermak J. E., (1986), "Wind Load Reduction for Heliostats", Solar Energy Research Institute Subcontract Report for the U.S. Department of Energy, SERI/STR-253-2859, May 1986, www.nrel.gov/docs/legosti/old/2859.pdf and http://www.osti.gov/bridge/product.biblio.jsp?osti_id=5556580

[4] Roos T. H., (2012), "A Wind Loading Correlation For An Isolated Square Heliostat, Part 2: Moments And Side Forces", Submitted to 1st South African Solar Energy Conference, Stellenbosch, South Africa, 21-23 May 2012